Microfluid Nanofluid (2007) 3:359–368
DOI 10.1007/s10404-007-0159-2

RESEARCH PAPER

A two-port model for wave propagation along a long circular microchannel

Timo Veijola

Received: 19 April 2006 / Accepted: 6 February 2007 / Published online: 8 March 2007

Abstract A compact model for oscillatory flow in a long microchannel with a circular cross-section is derived from the linearised Navier–Stokes equations. The resulting two-port model includes the effects of viscosity due to rarefied gas in the slip flow regime, inertia, compressibility and losses due to heat exchange. Both an acoustic impedance T network and an acoustic admittance Π network are presented for implementation in system level and circuit simulation tools. Also, reduced T and Π networks with constant component values are given to be used in the low frequency region. They are useful in time domain simulations, too. To verify the analytical model, simulations with a harmonic finite element solver for acoustic viscous flow are performed for microchannels exploiting the axisymmetry. The simulation results with both open and closed outlet conditions are compared with the two-port model with excellent agreement. Contribution of the slip conditions and the accuracy of the simple model are demonstrated.

Keywords Acoustic wave propagation · Slip flow · Microchannel · Compact model · Rarefied gas

1 Introduction

Gas-filled microchannels are an essential part of several micromechanical devices. The channels may transfer gas from one container to another, or the flow can be oscillatory. The measure for the oscillation frequency is the reduced frequency $k = \omega r_0/c_0$, where ω is the angular frequency, r_0 is the radius of the channel and c_0 is the speed of sound. If k approaches 0 and the flow velocity is relatively low, both steady and oscillatory flow can be modelled with linear flow resistances. It is typical for microchannels that their characteristic dimensions are comparable to the mean free path λ of the gas molecules. The measure of the rarefaction is the Knudsen number Kn. In the case of flow channels with circular cross sections, it is the relation between the mean free path λ and the radius of the flow channel r_0. Models for circular microchannels in the rarefied gas regime were studied from the beginning of the twentieth century by Knudsen (1909) and more recently by Sharipov and Seleznev (1998) and Karniadakis and Beskok (2002), among several others.

When the reduced frequency $k \ll 1$, the flow can be considered mainly viscous, but the inertia of the gas introduces a complex, frequency-dependent part to the flow impedance. Lumped flow impedance models for open capillaries with inertial effects have been studied in the literature in the continuum flow regime by Thurston (1952), Morris and Forster (2004), and in the transition flow regime by Hadjiconstantinou (2001).

When the reduced frequency $k > 1$, the channel behaves rather as an acoustic wave guide than a viscous flow channel. A transmission-line type two-port is needed to model the flow in the channel. The model for a long, circular acoustic wave guide is well discussed in the literature. The classical model that includes effects of viscosity and heat conduction on the acoustic propagation is based on the work by Stokes, Hemholtz and Kirchhoff in the nineteenth century. Several useful approximations were published by Rayleigh (1945), Daniels (1950), Beltman (1999), and Scheichl (2004) among several others. All these papers discuss the continuum flow regime only. Beltman (1999)

T. Veijola (✉)
Department of Electrical and Communications Engineering,
Helsinki University of Technology,
P.O. Box 3000, 02015 TKK, Finland
e-mail: timo.veijola@tkk.fi

presents a general viscothermal propagation model for various flow geometries, including the pressure-driven and moving-surfaces (squeezed-film damping) cases.

This paper presents a microchannel model that contains the gas rarefaction effects and extends the lumped flow impedance model to frequencies where $k < 1$, but where the two-port model is necessary. A relatively long channel (end effects can be considerd negligible) with a circular cross-section is assumed. The resulting two-port flow impedance contains the gas rarefaction effects in the slip flow regime, losses due to viscosity and thermal conductivity, and inertial and compressibility effects. At small reduced frequencies the model reduces to the flow resistance of the viscous flow channel.

The model is derived by following the derivation of the low reduced-frequency model by Beltman (1999), but considering slip boundary conditions for the velocity and temperature on the walls of the channel. This extends the model to be valid both in the continuum flow region ($K_n < 0.001$) and in the slip flow region ($0.001 < K_n < 0.1$). The two-port (four-pole) model is presented as an electrical equivalent circuit with frequency-dependent circuit elements, similarly to Daniels (1950) and Beranek (1986). This model is usable in the frequency-domain analysis, but to enable transient simulations, too, a model with constant element (component) values is given.

In Sect. 2, the Beltman model is first extended by considering the slip flow conditions on the channel surfaces. A two-port acoustic impedance is derived to enable the modelling of the capillary with general inlet and outlet conditions. In Sect. 3, implementations of this impedance with electrical-equivalent T and Π networks are given. Simple models for short channel sections with constant component values are presented, too. In Sect. 4, the model is verified with finite element method (FEM) simulations of both closed and open-ended capillaries. Finally, in Sect. 5, the accuracy of the complete model and the simplified model is discussed. The importance of the slip conditions is also demonstrated.

2 Analytic model for a circular microchannel

A model of wave propagation in a circular capillary, including the effects of viscosity, inertia and compressibility, and gas rarefaction, is derived from the *low reduced-frequency model* (LRF model) by Beltman (1999). The geometry of the capillary is shown in Fig. 1.

2.1 Characteristic numbers

The behaviour of the flow in a narrow channel is described in the frequency domain by a few characteristic numbers. The Reynolds number Re (the square of the shear wave number s) is the ratio between inertial and viscous forces

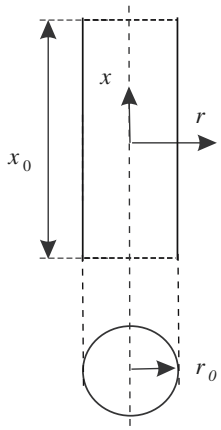

Fig. 1 Geometry of a circular capillary

$$s^2 = Re = \frac{\omega r_0^2 \rho_0}{\eta}, \tag{1}$$

where ω is the angular frequency, ρ_0 is the density of the gas, η is the viscosity coefficient, and r_0 is the radius of the channel.

The reduced frequency

$$k = \frac{\omega r_0}{c_0} \tag{2}$$

is scaled by r_0 and the speed of sound

$$c_0 = \sqrt{\frac{\gamma p_0}{\rho_0}}. \tag{3}$$

p_0 is the static pressure and γ is the specific heat ratio $\gamma = c_P/c_V$, where c_P and c_V are the specific heats at constant pressure and volume, respectively.

The Knudsen number $Kn = \lambda/r_0$ is a measure of gas rarefaction. It is the ratio between the mean free path λ and the radius r_0 of the channel. In this paper, the quantity

$$K_c = \frac{\sigma_p \lambda}{r_0} \tag{4}$$

is used as a measure of the rarefaction instead of Kn.

For the diffuse-specular scattering model, σ_p is specified by Sharipov and Seleznev (1998) as

$$\sigma_p = \frac{2-\alpha}{\alpha}[1.016 - 0.1211(1-\alpha)], \tag{5}$$

where α is the momentum accommodation coefficient. For diffuse scattering, $\alpha = 1$ and σ_p reduces to 1.016. Since λ is inversely proportional to pressure, K_c increases when the pressure drops below the ambient pressure.

Here the square root of the Prandtl number Pr is used to characterise the thermal properties

$$\phi = \sqrt{Pr} = \sqrt{\frac{\eta C_p}{\kappa}}, \tag{6}$$

where κ is the thermal conductivity.

K_T is the *thermal Knudsen number* specified by Karniadakis and Beskok (2002) as

$$K_T = \frac{2-\alpha_T}{\alpha_T}\left[\frac{2\gamma}{\gamma+1}\right]\frac{\lambda}{\phi^2 r_0}, \tag{7}$$

where α_T is the energy accommodation coefficient.

The collision frequency ε of the gas molecules depend on the average molecular velocity v_{ave} and the mean free path λ Park et al. (2004)

$$\epsilon = \frac{v_{ave}}{\lambda}, \tag{8}$$

where

$$v_{ave} = \sqrt{\frac{8k_B T_0}{\pi m}}, \tag{9}$$

and k_B is the Boltzmann coefficient ($k_B = 1.38 \times 10^{-23}$ J/K), m is the molecular mass, and T_0 is the temperature. The model derived in this paper assumes an infinite collision frequency.

2.2 Normalised variables

The variables $\bar{v}_x, \bar{p}, \bar{T}$, and $\bar{\rho}$ are the velocity, pressure, temperature, and density, respectively. The normalised variables are specified as

$$\begin{aligned} \bar{v}_x &= c_0 v_x e^{i\omega t}, \\ \bar{p} &= p_0(1 + pe^{i\omega t}), \\ \bar{T} &= T_0(1 + Te^{i\omega t}), \\ \bar{\rho} &= \rho_0(1 + \rho e^{i\omega t}) \end{aligned} \tag{10}$$

The spatial variables in the propagation and in the radial direction are $\bar{x}$ and $\bar{r}$, respectively. The normalised variables are specified as

$$x = \omega\bar{x}/c_0, \quad r = \bar{r}/r_0. \tag{11}$$

These definitions are identical to the ones used by Beltman (1999).

2.3 Low reduced frequency viscoelastic wave propagation model

The LRF model is applied here to a pressure-driven flow in a channel with a circular cross-section. The starting point is the set of general LRF equations, Eq. 24 in Beltman (1999). After applying the operators specified in Appendix A2 by Beltman, and considering the axial symmetry and non-moving channel walls (radial velocity is zero), the low reduced-frequency equations become

$$iv_x = -\frac{1}{\gamma}\frac{\partial p}{\partial x} + \frac{1}{s^2}\left(\frac{\partial^2 v_x}{\partial r^2} + \frac{1}{r}\frac{\partial v_x}{\partial r}\right), \tag{12}$$

$$0 = -\frac{1}{k\gamma}\frac{\partial p}{\partial r}, \tag{13}$$

$$\frac{\partial v_x}{\partial x} + ik\rho = 0, \tag{14}$$

$$p = \rho + T, \tag{15}$$

$$iT = \frac{1}{s^2\phi}\left(\frac{\partial^2 T}{\partial r^2} + \frac{1}{r}\frac{\partial T}{\partial r}\right) + i\left[\frac{\gamma-1}{\gamma}\right]p. \tag{16}$$

2.4 Slip boundary conditions

In the continuum flow regime both the velocity and the temperature are zero at the channel walls. When the non-zero mean free path is considered, the velocity and temperature have non-zero values at the walls. In the slip flow regime, the first-order boundary conditions are those given by Karniadakis and Beskok (2002) for velocity,

$$v_x(r=1) = -K_c \left.\frac{\partial v_x}{\partial r}\right|_{r=1}, \tag{17}$$

and temperature,

$$T(r=1) = -K_T \left.\frac{\partial T}{\partial r}\right|_{r=1}. \tag{18}$$

K_c and K_T are specified in Eqs. 4 and 7, respectively.

2.5 Solution for v_x and T

The pressure is a function of x only, and the velocity and temperature can be solved from Eqs. 12 and 16, respectively. Since these differential equations and the boundary conditions in Eqs. 17 and 18 have identical forms, the solution can be presented using a single function A. The solution for velocity can be written as

$$v_x = -\frac{i}{\gamma}A(s, K_c, r)\frac{\partial p}{\partial x} \tag{19}$$

and for temperature as

$$T = -\left[\frac{\gamma - 1}{\gamma}\right] pA(s\phi, K_T, r), \tag{20}$$

where the function A is

$$A(s, K_c, r) = \frac{I_0(s\sqrt{i}r)}{I_0(s\sqrt{i}) + \sqrt{i}K_c s I_1(s\sqrt{i})} - 1, \tag{21}$$

where I_0 and I_1 are the modified Bessel functions of the first kind. If $K_c = 0$, Eq. 21 reduces to the result in Appendix A2 in Beltman (1999).

2.6 Function B

After solving the function A with slip boundary conditions, the solution strategy by Beltman can be followed: the velocity, density and temperature in Eqs. 19, 15 and 20, respectively, are substituted into the equation of continuity, Eq. 14, resulting in

$$-\frac{iA(s, K_c, r)}{\gamma}\frac{\partial^2 p}{\partial x^2} + ikp\left[1 + \frac{\gamma - 1}{\gamma}A(s\phi, K_T, r)\right] = 0. \tag{22}$$

In the two-port model the average velocity through the cross-section is needed rather than the radial velocity distribution. Integrating across the cross-section of the channel gives the final wave equation for pressure. Since only the functions A depend on radius r, they are replaced with functions B that represent the average value of A

$$B(s, K_c) = \frac{1}{\pi}\int_0^1 A(s, K_c, r) 2\pi r \, dr. \tag{23}$$

This results in

$$B(s, K_c) = \frac{2I_1(s\sqrt{i})}{s\sqrt{i}I_0(s\sqrt{i}) + iK_c s^2 I_1(s\sqrt{i})} - 1. \tag{24}$$

The same result applies to $B(s\varphi, K_T)$.

2.7 Wave equation

After replacing functions A with functions B in Eq. 22, the resulting equation for the pressure distribution is

$$k^2\frac{\partial^2 p}{\partial x^2} - k^2\Gamma^2 p = 0, \tag{25}$$

where

$$\Gamma = \sqrt{\frac{\gamma}{n_\gamma(s\phi)B(s, K_c)}} \tag{26}$$

and

$$n_\gamma(s\phi) = \left[1 + \frac{\gamma - 1}{\gamma}B(s\phi, K_T)\right]^{-1}. \tag{27}$$

The polytrophic constant n_γ relates density and pressure. It affects mainly the spring forces due to the gas compressibility, but it introduces losses also. The polytrophic constant depends on the heat conduction and temperature boundary conditions. Here, isothermal walls with temperature jump conditions due to the rarefied gas are assumed. The value of the polytropic constant n_γ is between 1 (isothermal process, low-frequency region, and a small gap) and the specific-heat ratio γ (adiabatic process, high-frequency region, large gap).

2.8 Relative flow rate coefficient

At small frequencies the function $B(s,0)$ approaches $-is^2/8$, and its use in the following impedance equations is not very informative. An alternative variable, the relative flow rate coefficient Q_{pr}, is used here instead in the following equations. It is specified as

$$Q_{pr} = -\frac{8B(s, K_c)}{is^2}. \tag{28}$$

An approximation valid for small s is

$$Q_{pr,0} = \frac{1 + 4K_c}{1 + is^2\dfrac{1 + 6K_c + 12K_c^2}{6(1 + 4K_c)}}. \tag{29}$$

2.9 Denormalised wave equation for a pressure driven channel

The wave equation Eq. 25 is presented in a denormalised form as

$$\frac{\partial^2 \overline{p}(\overline{x}, \omega)}{\partial \overline{x}^2} - q^2\overline{p}(\overline{x}, \omega) = 0, \tag{30}$$

where the propagation coefficient q is specified as

$$q^2 = \frac{8i\omega\eta}{r_0^2 Q_{pr} p_0 n_\gamma(s\phi, K_T)}. \tag{31}$$

The pressure function satisfying Eq. 30 is

$$\overline{p}(\overline{x}, \omega) = C_1 e^{q\overline{x}} + C_2 e^{-q\overline{x}}, \tag{32}$$

where C_1 and C_2 are constants to be determined from the boundary conditions at the ends of the channel. Setting boundary conditions $\overline{p}(-x_0/2, \omega) = \overline{p}_1$ and $\overline{p}(x_0/2, \omega) = \overline{p}_2$, the pressure distribution along the channel is

$$\overline{p}(\overline{x},\omega) = -\frac{\overline{p}_1 e^{-qx_0/2} - \overline{p}_2 e^{qx_0/2}}{e^{qx_0} - e^{-qx_0}} e^{q\overline{x}} + \frac{\overline{p}_1 e^{qx_0/2} - \overline{p}_2 e^{-qx_0/2}}{e^{qx_0} - e^{-qx_0}} e^{-q\overline{x}}. \quad (33)$$

2.10 Two-port impedance

To have a simulation model, the relations between pressures and velocities at both channel ends should be solved. Here, volume velocities are used so that these can be expressed via acoustic impedances.

Equation 19 gives the relation between the velocity and pressure in the propagation direction. After denormalising and averaging the velocity across the cross-section, the averaged velocity is

$$\overline{v}_x(\overline{x}) = -\frac{r_0^2 Q_{pr}}{8\eta}\frac{\partial \overline{p}(\overline{x},\omega)}{\partial \overline{x}}. \quad (34)$$

The volume velocities at the inlet and outlet are $\overline{U}_1 = \pi r_0^2 \overline{v}_x(-x_0/2)$ and $\overline{U}_2 = -\pi r_0^2 \overline{v}_x(x_0/2)$. We can write

$$\begin{bmatrix} \overline{p}_1 \\ \overline{p}_2 \end{bmatrix} = \begin{bmatrix} Z_{A11} & Z_{A12} \\ Z_{A21} & Z_{A22} \end{bmatrix} \begin{bmatrix} \overline{U}_1 \\ \overline{U}_2 \end{bmatrix}, \quad (35)$$

where Z_{Aij} are the acoustic impedances that can be solved using the volume velocities specified above and from Eq. 34, resulting in

$$\begin{bmatrix} \overline{p}_1 \\ \overline{p}_2 \end{bmatrix} = Z_{A0} \begin{bmatrix} \frac{1}{\tanh(qx_0)} & \frac{1}{\sinh(qx_0)} \\ \frac{1}{\sinh(qx_0)} & \frac{1}{\tanh(qx_0)} \end{bmatrix} \begin{bmatrix} \overline{U}_1 \\ \overline{U}_2 \end{bmatrix}, \quad (36)$$

where

$$Z_{A0} = \frac{8\eta}{\pi r_0^4 q Q_{pr}} \quad (37)$$

is the characteristic acoustic impedance of the flow channel. Equation 36 describes an acoustic transmission line, analogous to the electrical one discussed by Gardiol (1987). At high frequencies Z_{A0} approaches a constant, real value of $\rho_0 c_0/(\pi r_0^2)$ that contains the specific acoustic impedance of free space ($\rho_0 c_0$).

Equation 36 can be used to calculate the characteristics of the capillary, as long as two variables from $\overline{p}_1, \overline{p}_2, \overline{U}_1$, and $\overline{U}_2$ are fixed. Assume that port 2 in the capillary is terminated with an impedance Z_{A2}. The impedance at port 1 is then

$$Z_{A1} = Z_{A0}\frac{Z_{A2} + Z_{A0}\tanh(qx_0)}{Z_{A0} + Z_{A2}\tanh(qx_0)}. \quad (38)$$

The most important characteristics are the open and closed channel impedances Z_{Aopen} and $Z_{Aclosed}$, respectively:

$$Z_{Aopen} = \left.\frac{\overline{p}_1}{\overline{U}_1}\right|_{\overline{p}_2=0} = Z_{A0}\tanh(qx_0), \quad (39)$$

$$Z_{Aclosed} = \left.\frac{\overline{p}_1}{\overline{U}_1}\right|_{\overline{U}_2=0} = \frac{Z_{A0}}{\tanh(qx_0)}. \quad (40)$$

2.11 Distributed impedance and admittance

The distributed longitudinal impedance z_{AS} and the transversal admittance y_{AP} per unit length are solved from the equations for the characteristic impedance $Z_{A0} = \sqrt{z_{AS}/y_{AP}}$ and the propagation factor $q = \sqrt{z_{AS} z_{AP}}$.

$$z_{AS} = qZ_{A0} = \frac{8\eta}{\pi r_0^4 Q_{pr}}, \quad (41)$$

$$y_{AP} = \frac{q}{Z_{A0}} = \frac{i\omega\pi r_0^2}{p_0 n_\gamma(s\phi, K_T)}. \quad (42)$$

Approximations at low frequencies can be obtained by writing the Taylor series for these distributed impedances. The approximated distributed longitudinal impedance and transverse admittance, respectively, are

$$z_{AS} \approx \frac{8\eta}{\pi r_0^4(1+4K_c)} + i\omega\frac{4\rho_0(1+6K_c+12K_c^2)}{3\pi r_0^2(1+4K_c)^2} \quad (43)$$

and

$$y_{AP} \approx \frac{1}{\frac{p_0}{i\omega\pi r_0^2} + \frac{\rho_0 p_0 c_P}{8\pi\gamma\kappa}(\gamma-1)(1+4K_T)}. \quad (44)$$

3 Electrical equivalent circuit implementations

There are several alternative ways to implement the mechanical-impedance two-port specified in Eq. 36.

Here, T- and Π-network realisations are presented that can be used to calculate the accurate response for all inlet/outlet impedance conditions. Also, simple low-order approximations modelling short line sections with frequency-independent component values are presented for both realisations.

These networks are usable in building models for circuit simulation and system simulation programs. With these tools, frequency responses and time-domain responses for arbitrary inlet/outlet impedances or networks can be calculated.

3.1 T network

The T-equivalent acoustic impedance circuit is shown in Fig. 2a. The accurate values and short-line approximations for the series impedances and parallel admittances, respectively, are

$$Z_{\mathrm{AS}} = Z_{\mathrm{A0}} \tanh(qx_0/2) \approx \frac{R_{\mathrm{A1}}}{2} + \frac{\mathrm{i}\omega L_{\mathrm{A1}}}{2} \tag{45}$$

and

$$Z_{\mathrm{AP}} = \frac{Z_{\mathrm{A0}}}{\sinh(qx_0)} \approx \frac{1}{G_{\mathrm{A1}}} + \frac{1}{\mathrm{i}\omega C_{\mathrm{A1}}}. \tag{46}$$

The approximate lumped component values for a short section of length l are

$$R_{\mathrm{A1}} = \frac{8\eta l}{\pi r_0^4 (1 + 4K_c)}, \tag{47}$$

$$L_{\mathrm{A1}} = \frac{4\rho_0(1 + 6K_{\mathrm{c}} + 12K_{\mathrm{c}}^2)l}{3\pi r_0^2 (1 + 4K_{\mathrm{c}})^2}, \tag{48}$$

$$C_{\mathrm{A1}} = \frac{\pi r_0^2 l}{p_0}, \tag{49}$$

and

$$G_{\mathrm{A1}} = \frac{8\pi\gamma\kappa l}{\rho_0 p_0 c_{\mathrm{P}}(\gamma - 1)(1 + 4K_{\mathrm{T}})}. \tag{50}$$

Figure 2b shows the approximating circuit. Capacitance C_{A2} has been added to correct the high-frequency response. At high frequencies the capacitance of the parallel section approaches C_{A1}/γ. This results in

$$C_{\mathrm{A2}} = \frac{C_{\mathrm{A1}}}{\gamma - 1}. \tag{51}$$

Several sections of the simple model can be cascaded to improve the accuracy of the approximation at high frequencies. In this case $l = x_0/N$, where N is the number of sections.

3.2 Π network

An alternative way to construct the equivalent circuit is to use an acoustic-admittance ($Y_{\mathrm{A}} = 1/Z_{\mathrm{A}}$) Π network, as shown in Fig. 3.

The series admittance and the admittances in the parallel branches, respectively, are

$$Y_{\mathrm{AS}} = \frac{1}{Z_{\mathrm{A0}} \sinh(qx_0)} \approx \frac{1}{R_{\mathrm{A1}} + \mathrm{i}\omega L_{\mathrm{A1}}} \tag{52}$$

and

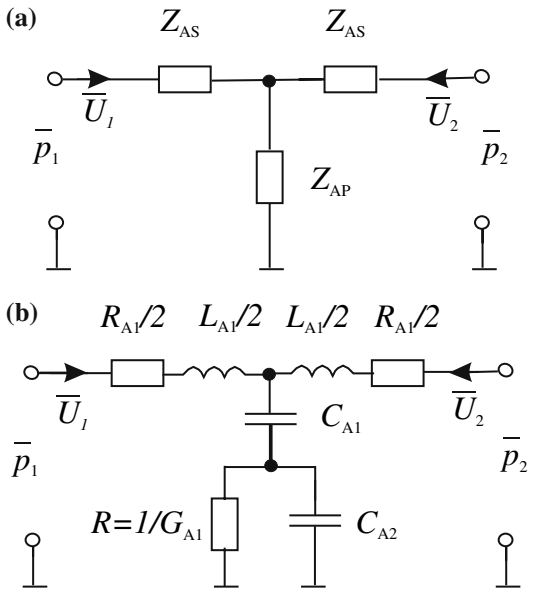

Fig. 2 T networks for calculating the acoustic impedance characteristics of a circular flow channel. **a** An accurate model with frequency-dependent acoustic impedances, and **b** a small-frequency approximation for a short line section of the channel with constant component values

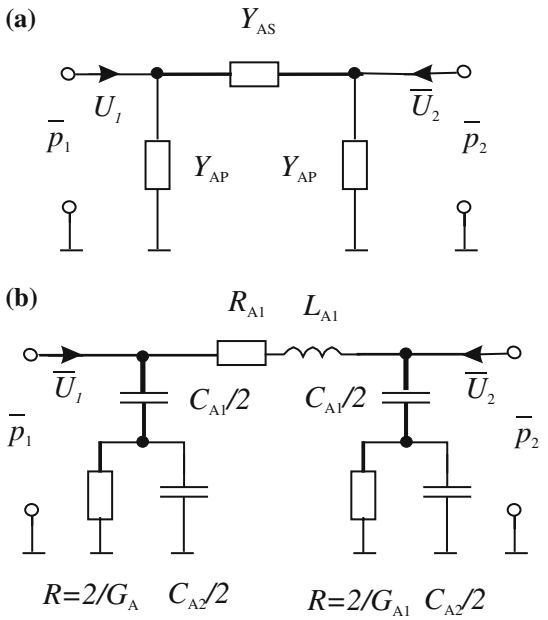

Fig. 3 Π networks for calculating the acoustic impedance characteristics of a circular flow channel. **a** An accurate model with frequency-dependent acoustic admittances, and **b** a small-frequency approximation for a short line section with constant component values

$$Y_{\mathrm{AP}} = \frac{\tanh(qx_0/2)}{Z_{\mathrm{A0}}} \approx \frac{1}{\dfrac{2}{G_{\mathrm{A1}}} + \dfrac{2}{\mathrm{i}\omega C_{\mathrm{A1}}}}. \quad (53)$$

The component values in Eqs. 47–50 for the approximate T network are the same as for the Π network. Also, additional capacitances $C_{\mathrm{A2}}/2$ have been added to the circuit to correct the frequency response when n_γ approaches infinity.

The Π network is suited for approximating an input impedance of an open-ended channel (that is, port 2 of the equivalent circuit is short-circuited).

The components in the simple equivalent circuits clearly show the equivalency with electrical transmission lines: the series resistances and inductances are due to gas viscosity and inertia, respectively. The parallel capacitances and conductances model the spring effect and losses due to compressibility, respectively.

4 FEM simulations

To verify the results derived FEM simulations were performed. Impedances for capillaries with open or closed ends were simulated and compared with the model. A solver for dissipative acoustic equations in a multiphysical FEM software Elmer (2006) was used. The dissipative-acoustics equations were discretised using enhanced MINI finite elements while residual free bubbles were used for the Navier–Stokes equation by Malinen et al. (2004). The methods ensure good numerical behaviour but have a high computational cost. The circuit simulation and design tool Aplac (2006) was used to calculate the responses of the electrical equivalent circuits.

Figure 4 shows the axisymmetric simulation space with encircled boundaries. Slip conditions were assumed for boundary 2 with the $T = 0$ condition. The simulated acoustic impedance Z_{AFEM} is calculated from the average of the pressure p_1 divided by the volume velocity on boundary 1.

Parameters for air at ambient pressure are used in the simulations. The numerical values are shown in Table 1. A mesh of 5,000 elements was used, and the number of simulated frequencies was 65.

4.1 Capillary with an open end

The acoustic impedance of an open capillary was first simulated. In the FEM simulations, pressures $\overline{p}_1$ and $\overline{p}_2$ at boundaries 1 and 3 (ports 1 and 2, respectively) were set to 1 Pa and 0 Pa, respectively, and the volume velocity $\overline{U}_1$ at port 1 was calculated from the velocity distribution. These conditions ensured that there are no fringe effects at the ends of the capillary. Figure 5 shows both the simulated results and the analytic impedance Z_{Aopen} in Eq. 39 for two capillary geometries.

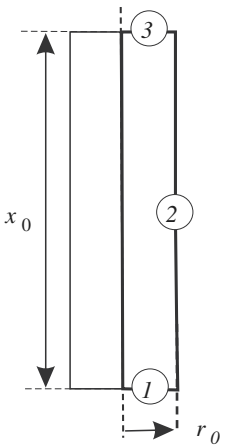

Fig. 4 Axisymmetric simulation space of a circular capillary

4.2 Capillary with a closed end

Next, the acoustic admittance of a closed capillary was simulated. In the FEM simulations, pressure $\overline{p}_1$ at port 1 was set to 1 Pa and the velocity at port 2 $\overline{U}_2$ was set to 0. The volume velocity $\overline{U}_1$ at port 1 was then calculated from the velocity distribution. Since the imaginary part of the impedance approaches infinity when the frequency approaches zero, an admittance response is shown instead of the impedance. Figure 6 shows both the simulated results and the analytic admittance $1/Z_{\mathrm{Aclosed}}$ specified in Eq. 40 for two capillary topologies. These figures show the real parts and the negation of the imaginary parts of the admittance.

5 Discussion

5.1 Accuracy of the analytic model

In principle, the analytic frequency responses should be exactly the same as those simulated with FEM tools. This

Table 1 Gas parameters used in simulations

Parameter	Description	Value	Unit
p_0	Pressure	101.3	10^3 N/m^2
T_0	Temperature	300	K
η	Viscosity coefficient	18.5	10^{-6} N s/m^2
λ	Mean free path	68.23	10^{-9} m
κ	Heat conductivity	25	10^{-3} W/m/K
ρ_0	Density	1.155	kg/m^3
c_{P}	Specific heat	1.01	10^3 J/kg/K
γ	Specific heat ratio $\gamma = c_{\mathrm{P}}/c_{\mathrm{V}}$	1.4	
α	Accommodation coefficient	1.0	
α_{T}	Thermal acc. coefficient	1.0	
m	Molecular mass	4.85	10^{-26} kg

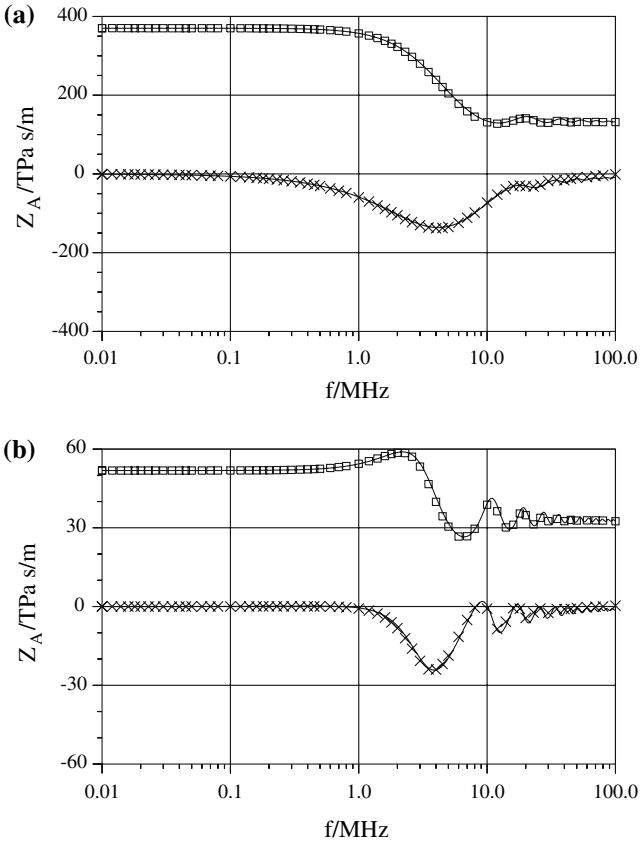

Fig. 5 Simulated real (*open square*) and imaginary (*multiplication symbol*) parts of the acoustic impedance of an open ended capillary in 10^{12} Pa s/m. Z_{Aopen} from the analytical expression is also shown (*solid line*). The dimensions of the capillary are **a** $r_0 = 1$ μm and $x_0 = 10$ μm and **b** $r_0 = 2$ μm and $x_0 = 20$ μm

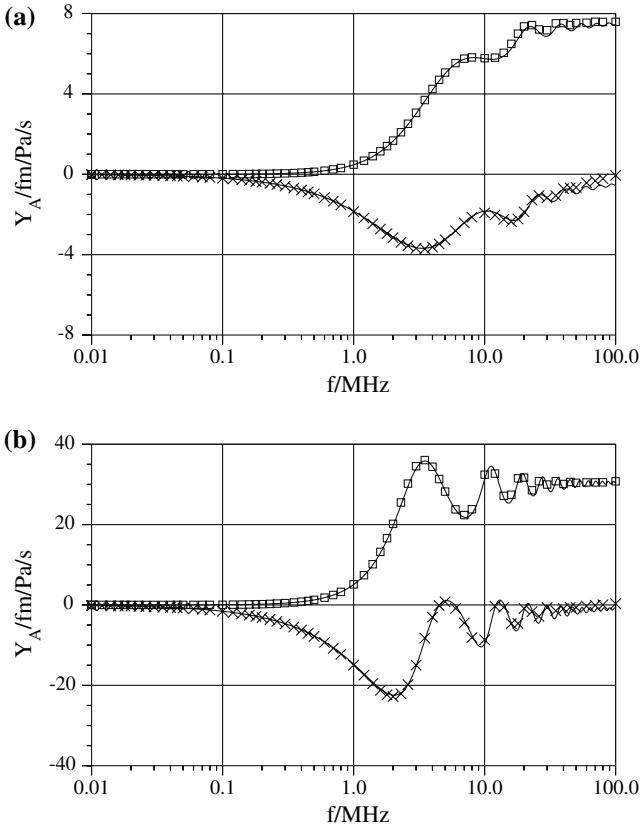

Fig. 6 Simulated real (*open square*) and negative of the imaginary (*multiplication symbol*) parts of the acoustic admittance for a closed-ended capillary in 10^{-15} m/s/Pa. $1/Z_{Aclosed}$ from the analytical expression is also shown (*solid line*). The dimensions of the capillary are **a** $r_0 = 1$ μm and $x_0 = 10$ μm and **b** $r_0 = 2$ μm and $x_0 = 20$ μm

is due to the fact that, in both cases, the solved equations are the same, and so are the boundary conditions. This is also a proof that the derived equations are correct. As Figs. 5 and 6 show, the agreement is excellent but not perfect. There are some differences in the high-frequency region.

In deriving this model, idealistic end-conditions were assumed. In practice, the fringe flows and acoustic radiation at the open ends should be considered for a more accurate model, especially for relatively short channels ($x_0/r_0 < 20$). Also, the closed end needs an end-correction since the flow profile at the closed end differs from the flow profile in the middle of a long channel. There are two ways to extend the validity of the present model for short channels. In the first one, the length of the tube with ideal end-conditions is simply extended to approximately compensate the end effects. The amount of the open-end correction depends on the output conditions. A published value for the end correction exists for small reduced frequency k. For continuum flow and for an unflanged end, the end correction is $0.6133r_0$ according to Levine and Schwinger (1948), and for a flanged end it is $0.68r_0$ as given by Weissberg (1962) and $3\pi/16r_0 \approx 0.59r_0$ by Sharipov and Seleznev (1998). The second way to extend the validity of the model is to use the presented equivalent circuit and connect to it an equivalent circuit modelling the end correction. In this way, both the correction due to the viscous flow (small k) and due to the inertia (attached mass) could be included in the model.

An infinite molecular collision frequency was assumed in the model and the FEM simulations. According to Eq. 8 and the parameters in Table 1, this frequency is 6.8 GHz. This is 68 times the maximum frequency used in the simulations.

5.2 Accuracy of the simple model

The simple model presents a short section of the flow channel and is valid only at low frequencies. For an improved model, several sections must be cascaded. The equivalent circuit with frequency-independent components can be simulated also in the time domain. The simple model is applicable also in environments where the com-

plex Bessel functions are not available. But how accurate is this simple model? This is a difficult question that has no simple answer. The only fact is that the approximation improves with the number of cascaded sections N. But, since functions Q_{pr} and n_γ, that specify the flow and temperature profiles in the channel, are approximated in the simple model, the response of the cascaded circuit never approaches the accurate impedance.

Figure 7 shows how the number of sections affects the response of the open-ended capillary. The responses for both T and Π networks are shown for $N = 2$ and $N = 8$. It is clear that the frequency range of the approximation is several orders wider for $N = 8$, but it is hard to make any judgments on whether the T- or Π-network approximation is better.

5.3 Slip conditions

A lot of work was done here in modelling the slip conditions. Is this work and the increased complexity of the model worth the trouble? Also, the effect of slip conditions is studied with a simulation example: the impedance of an open channel is compared with an impedance that is calculated assuming continuum boundary conditions ($\lambda = 0$), see Fig. 8.

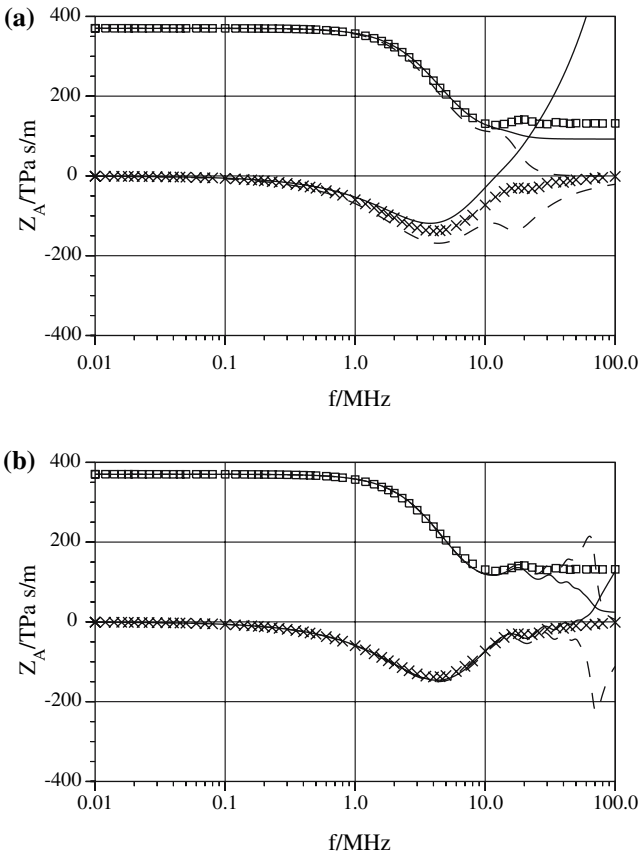

Fig. 7 The response of the simple T-network (*solid line*) and Π-network (*dashed line*) model of an open-ended capillary, when **a** two ($N = 2$) and **b** eight ($N = 8$) sections are used. The dimensions of the capillary are $r_0 = 1$ μm and $x_0 = 10$ μm. The real (*open square*) and imaginary (*multiplication symbol*) parts from the FEM simulation are shown for comparison

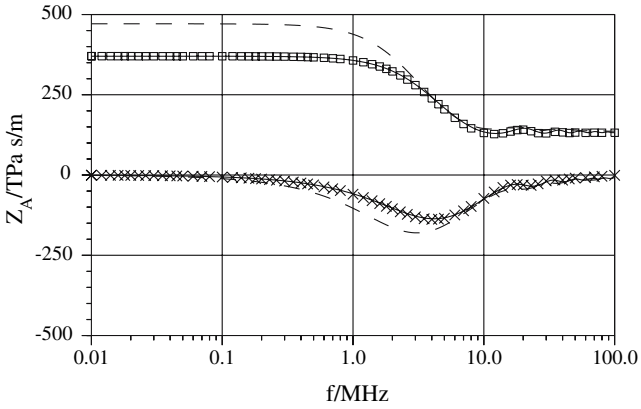

Fig. 8 Simulated real (*open square*) and imaginary (*multiplication symbol*) parts of the acoustic impedance of an open ended capillary. Z_{Aopen} from the analytic expression with slip conditions is shown (*solid line*) with the response of the model with continuum boundary conditions ($\lambda = 0$) (*dashed line*). The dimensions of the capillary are $r_0 = 1$ μm and $x_0 = 10$ μm

This demonstration shows that accounting for slip conditions is very important in channels with a radius of 1 μm or less. If the slip conditions are not included in the model, the impedance will be overestimated in the low-frequency region, in this case by about 30%.

6 Conclusions

A compact model for calculating the frequency-domain characteristics of long circular capillaries with micromechanical dimensions is presented. Two alternate electrical-equivalent circuit realisations for the acoustic impedance are given, namely the T- and Π-networks. Low-frequency circuits with constant component values are given for both cases, as well. The model was verified with FEM simulations with an excellent agreement, showing that the equations derived in this paper are valid.

The model has several applications in simulating oscillating micromechanical structures containing tiny flow channels. E.g., it is usable in calculating the characteristics of perforated gas dampers. The simplified circuits are usable also in transient simulations.

The model derived has idealistic boundary conditions and is not directly applicable to relatively short channels. However, using elongation models, the application range can be extended for channels of any length.

Acknowledgments The author wishes to thank Antti Pursula and Peter Råback for valuable help with Elmer FEM simulations and Luis Costa who has contributed to this publication by reading and checking the English language.

References

Aplac (2006) http://www.aplac.com
Beltman WM (1999) Viscothermal wave propagation including acousto-elastic interaction, part I: theory. J Sound Vib 227:555–586
Beranek LL (1986) Acoustics. American Institute of Physics, New York
Daniels FB (1950) On the propagation of sound waves in a cylindrical conduit. J Acoust Soc Am 22:563–564
Elmer (2006) Elmer—finite element solver for multiphysical problems. http://www.csc.fi/elmer
Gardiol FE (1987) Lossy transmission lines. Artech House, Norwood
Hadjiconstantinou NG (2001) Sound wave propagation in transition-regime micro- and nanochannels. Phys Fluids 14:802–809
Karniadakis GE, Beskok A (2002) Micro flows, fundamentals and simulation. Springer, Heidelberg
Knudsen M (1909) Ann Physik 28:75–130
Levine H, Schwinger J (1948) On the radiation of sound from an unflanged circular pipe. Phys Rev 73(4):383–406
Malinen M, Lyly M, Råback P, Kärkkäinen A, Kärkkäinen L (2004) A finite element method for the modeling of thermo-viscous effects in acoustics. In: Neittaanmäki P, Rossi T, Majava K, Pironneau O (eds) Proceedings of the 4th European congress on computational methods in applied sciences and engineering. Jyväskylä, Finland
Morris CJ, Forster FK (2004) Oscillatory flow in microchannels. Exp Fluids 36:928–937
Park JH, Bahukudumbi P, Beskok A (2004) Rarefaction effects on shear driven oscillatory gas flows: a direct simulation Monte Carlo study in the entire Knudsen regime. Phys Fluids 16:317–330
Rayleigh L (1945) The theory of sound. Dover, New York
Scheichl S (2004) On the calculation of the transmission line parameters for long tubes using the method of multiple scales. J Acoust Soc Am 115:534–555
Sharipov F, Seleznev V (1998) Data on internal rarefied gas flows. J Phys Chem Ref Data 27(3):657–706
Thurston GB (1952) Periodic fluid flow through circular tubes. J Acoust Soc Am 24:653–656
Weissberg HL (1962) End correction for slow viscous flow through long tubes. Phys Fluids 5(9):1033–1036